Available online at www.sciencedirect.com
ScienceDirect
Trans. Nonferrous Met. Soc. China 22(2012) s7−s13
Transactions of Nonferrous Metals Society of China
www.tnmsc.cn

Microstructure, tensile properties and fractography of A356 alloy under as-cast and T6 obtained with expendable pattern shell casting process

JIANG Wen-ming[1, 2], FAN Zi-tian[1], LIU De-jun[1]

1. State Key Laboratory of Material Processing and Die & Mould Technology, Huazhong University of Science and Technology, Wuhan 430074, China;
2. School of Mechanical & Electrical Engineering, Wuhan Institute of Technology, Wuhan 430073, China

Received 9 July 2012; accepted 30 August 2012

Abstract: The microstructure, tensile properties and fractography of A356 alloy were studied under as-cast and T6 conditions obtained with expendable pattern shell casting, and the results were compared with lost foam casting (LFC). The results indicate that α(Al) primary, eutectic silicon and Mg_2Si are the main phases in the microstructure of A356 alloy obtained with this casting process. The eutectic silicon particles are spheroidized and uniformly distributed at the grain boundaries after T6 treatment. The average length, average width and aspect ratio of eutectic silicon particles after T6 condition decrease. The sizes of *α*(Al) primary phase and eutectic silicon of this casting process are smaller than those of LFC. The tensile strength, elongation and hardness of A356 alloy after T6 obviously increase, they reach 260.53 MPa, 6.15% and 86.0, respectively and have a significant improvement compared to LFC. The fracture surfaces of expendable pattern shell casting show a mixed quasi-cleavage and dimple fracture morphology as a transgranular fracture nature. However, the fracture surfaces of LFC display a brittle fracture.

Key words: A356; microstructure; tensile properties; fracture surface; dimple fracture; brittle fracture; expendable pattern shell casting

1 Introduction

Nowadays, large-size, complicated and thin-walled aluminum alloy precision castings are extensively applied in the aerospace and automotive industries due to its excellent castability, corrosion resistance as well as high strength to weight ratio, etc [1−3]. However, the casting processes, which usually produce aluminum alloy castings, are difficult to reach the requirements of large-size, complicated, thin-walled and high quality, etc. Today, the lost foam casting (LFC) has been regarded as a near net shape method for manufacturing complicated aluminum and magnesium alloys precision castings [4−6]. However, the decomposition of the foam pattern during the pouring process may result in porosity and slag inclusion defects [7,8], and the pouring temperature of LFC is usually higher than that of traditional cavity casting. As a result, the coarser grains, serious porosity defects and poor mechanical properties are main problems for LFC.

This work introduced a compound casting process named expendable pattern shell casting process to improve the production of the complicated and thin-walled aluminum alloy precision castings and solve the problems involved in the casting processes reviewed above. This compound casting process combines the foam pattern preparation of LFC, thin shell precision fabrication of investment casting as well as vacuum pouring. It has the following advantages: flexible design of size and structure of parts, low cost of the foam pattern, high precision of ceramic shell and better filling ability of vacuum pouring. In the previous studies [9−11], this casting process mainly focused on the ferrous alloys casting, however, aluminum alloy was not involved. The authors introduce this compound casting process to casting aluminum alloy. In the present work, the microstructure, tensile properties and fractography of A356 aluminum alloy with as-cast and T6 heat treatment obtained with expendable pattern shell casting process were studied and compared with LFC.

Foundation item: Project (51204124) supported by the National Natural Science Foundation of China; Project (2012M511610) supported by the China Postdoctoral Science Foundation; Project (14125041) supported by the Scientific Research Foundation of Wuhan Institute of Technology
Corresponding author: JIANG Wen-ming; Tel: +86-13871264655, +86-027-87540094; E-mail: jwenming@163.com

2 Experimental

Figure 1 shows the schematic diagram of expendable pattern shell casting process. The foam patterns were first prepared using the foaming molding technology. The ceramic shell was then produced using coating the foam patterns with the ceramic slurry and using refractory to form the stucco on the coated patterns. Firstly, the ceramic shell prepared was placed inside a sand box. The sand box was then filled with 40/50 unbonded loose-sand. The loose-sand was compacted using a three-dimensional vibration table, and the sand box was then covered with a plastic film.

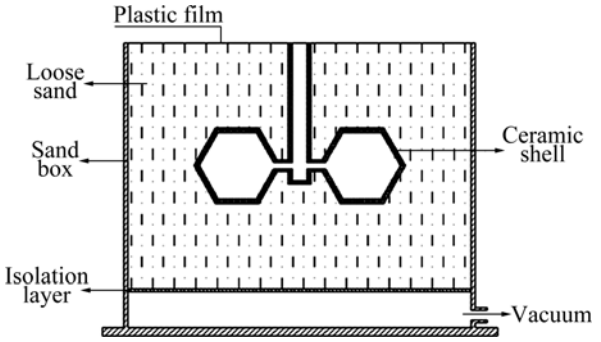

Fig. 1 Schematic diagram of expendable pattern shell casting process

Table 1 represents the chemical composition of A356 aluminum alloy used in this study. The crucible was first preheated, and the preheated aluminum ingot was placed inside the crucible. The Al-10%Sr master alloy was added to the molten melt at 730 °C. The molten metal was refined using argon gas as the temperature reached 750 °C, and the slag was then skimmed. Finally, the molten metal was ready for pouring process. The vacuum used in this study was 0.02 MPa. Meanwhile, A356 aluminum alloy was also produced by LFC under the same experimental conditions aiming at the comparisons of microstructure, tensile properties and fractography of expendable pattern shell casting process and LFC.

Table 1 Chemical composition of A356 alloy (mass fraction, %)

Si	Mg	Ti	Fe	Sr	Al
7.10	0.31	0.23	0.17	0.05	Bal.

Figure 2 presents the shape and dimensions of tensile specimens. The T6 heat treatment includes solution treatment and aging treatment. The solution treatment was firstly carried out at 538 °C for 12 h, and then quenched into hot water at 80 °C. The aging treatment was then performed at 165 °C for 6 h. Tensile tests were carried out using a WE-100 universal testing machine at room temperature with a 2 mm/min stretching rate. The hardness of A356 aluminum alloy was measured using a HB-3000 hardness test machine.

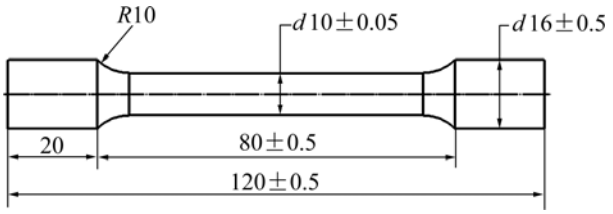

Fig. 2 Shape and dimensions of tensile specimens (Unit: mm)

The metallographic samples were cut from the end of tensile specimens. The metallographic samples were etched using 0.5% hydrofluoric acid solution after polishing. Microstructures were observed by using a Me F-3 metallographic microscope. The secondary dendrite arm spacing (SDAS), average length and average width of silicon particles were measured using an ImageTool metallographic analysis software. The aspect ratio of silicon particles was the ratio of average length of silicon particles and average width of silicon particles. The grains sizes of α(Al) primary phase were calculated according to the following equation:

$$D = 2\sqrt{A/\pi} \quad (1)$$

where A is the average area of α(Al) primary phase, which is also measured using the ImageTool software.

The fractured surfaces of tensile samples were observed using a QUAN TA-400 scanning electron microscope (SEM).

3 Results and discussion

3.1 Microstructure

Figures 3 and 4 indicate the microstructures of A356 aluminum alloy with as-cast and T6 produced by expendable pattern shell casting and LFC (Lost foam casting), respectively. Figure 5 shows the microstructures of the eutectic zone under as-cast and T6 conditions to demonstrate a substantial microstructure difference in the size and shape of eutectic silicon particles. A356 aluminum alloy as a hypoeutectic alloy firstly begins with growth of α(Al) primary phase and Al-Si eutectic between the dendrite arms during solidification process [12]. Meanwhile, Mg_2Si phase are also precipitated during solidification. As shown in Figs. 3 and 4, it is evident that the white phase is α(Al) primary phase, which exhibits the dendrite morphology, and the grey phases are Al-Si eutectic in the grain boundary no matter as-cast condition or T6 condition. Moreover, the large porosity defects in microstructure obtained with LFC can be observed because of the decomposition of the foam

pattern during pouring, as shown in Fig. 4. While the microstructure obtained with expendable pattern shell casting are denser because the foam pattern has been removed before pouring. In addition, it can be seen that the finer eutectic silicon particles are distributed in the grain boundary due to the better modification ability of Sr. However, some plate-like eutectic silicon particles can also be observed in the as-cast sample, as shown in Fig. 5(a). The eutectic silicon particles are spheroidized and homogeneously distributed in the grain boundary

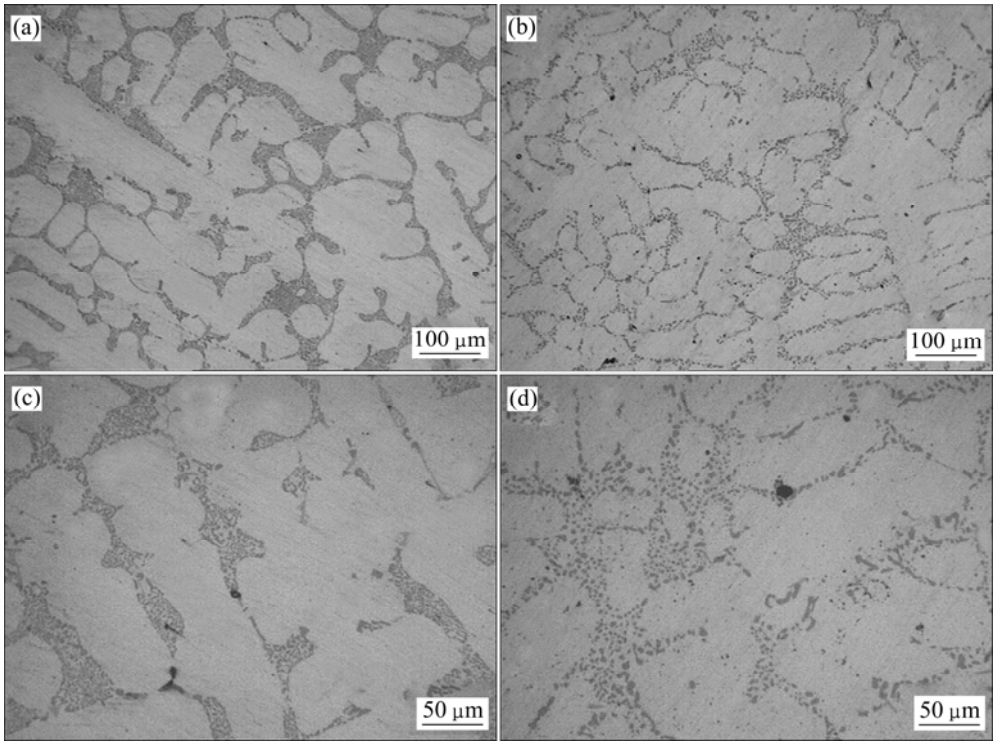

Fig. 3 Microstructures of A356 aluminum alloy obtained with expendable pattern shell casting: (a) Low magnification of as-cast; (b) Low magnification of T6; (c) High magnification of as-cast; (d) High magnification of T6

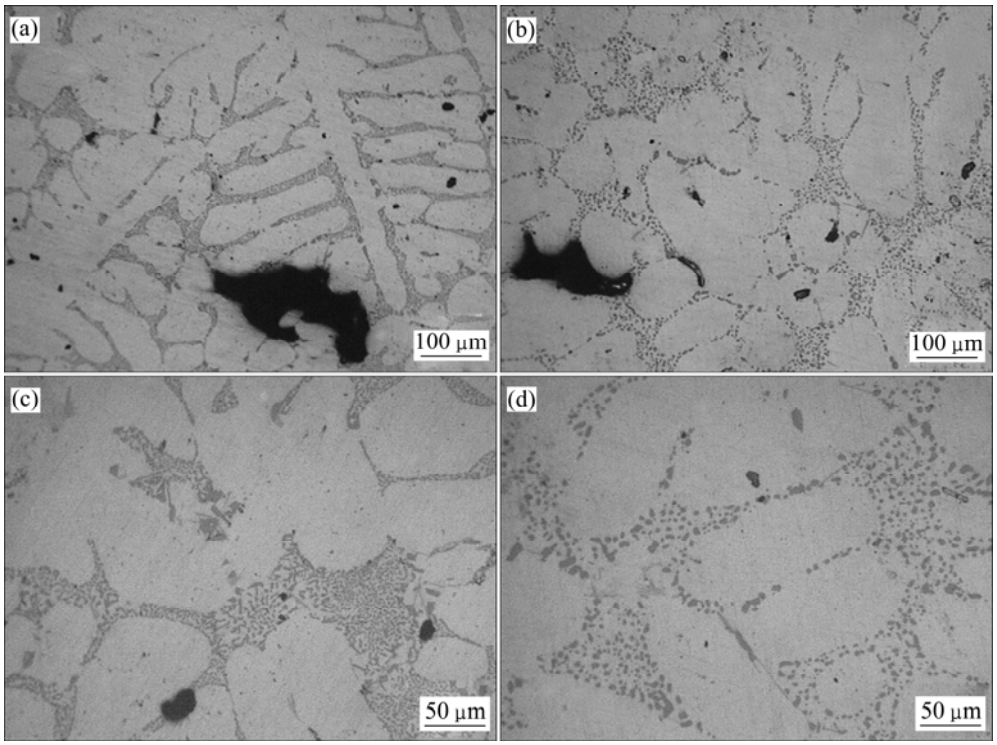

Fig. 4 Microstructures of A356 aluminum alloy obtained with LFC: (a) Low magnification of as-cast; (b) Low magnification of T6; (c) High magnification of as-cast; (d) High magnification of T6

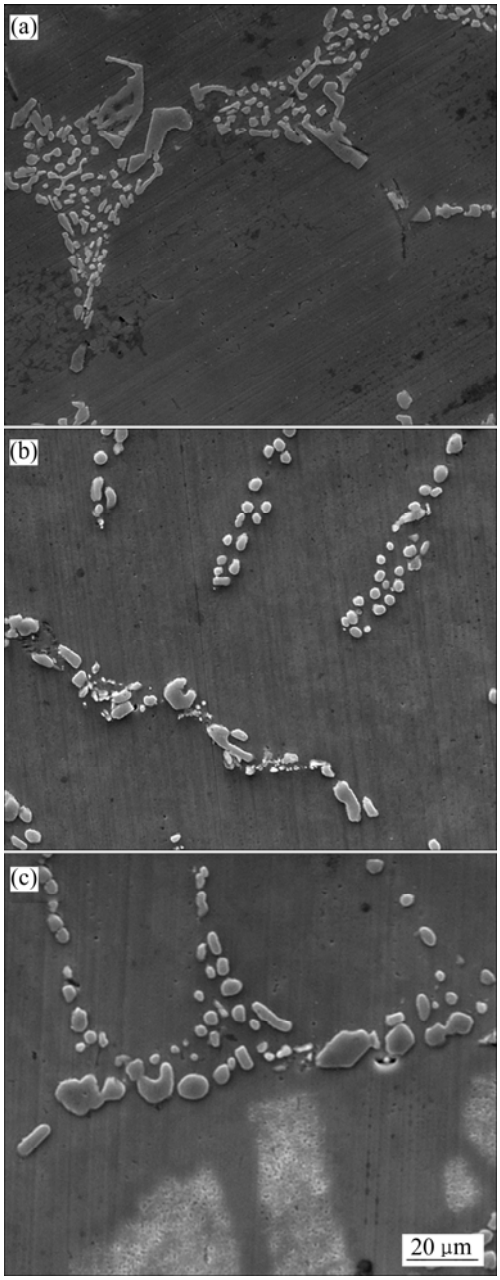

Fig. 5 Morphology of eutectic silicon of A356 aluminum alloy obtained with: (a) as-cast of expendable pattern shell casting; (b) T6 of expendable pattern shell casting; (c) T6 of LFC

after T6 heat treatment, as shown in Fig. 5(b). For the comparison, the sizes of eutectic silicon particles of LFC obviously increase compared to expendable pattern shell casting, as shown in Fig. 5(c).

Table 2 shows the quantitative metallography results of microstructure features including α(Al) primary phase and eutectic silicon particles of A356 aluminum alloy obtained with expendable pattern shell casting and LFC. It can be seen that the size of α(Al) primary phase and SDAS value under as-cast condition are slightly smaller than that of T6 condition. However, the average length, average width and aspect ratio of eutectic silicon particles under T6 condition greatly decrease compared to as-cast condition, and the morphology of eutectic silicon particles looks more round. Furthermore, the sizes of α(Al) primary phase and eutectic silicon particles in microstructure of expendable pattern shell casting obviously decrease compared to LFC, especially in aspect ratio of silicon particles.

Figure 6 represents the cooling curve of the molten metal during solidification for the different casting processes. It is evident that the cooling rate obtained using the expendable pattern shell casting is faster than that of LFC. This can be explained by the fact that the heat dissipation of dry sand used in the LFC is low. As a result, the faster cooling rate of the expendable pattern shell casting brings about a significant improvement in the microstructure compared to LFC.

3.2 Tensile properties

Table 3 presents the tensile strength, elongation and hardness of A356 aluminum alloy with as-cast and T6 obtained by expendable pattern shell casting and LFC. It is evident that the tensile strength, elongation and hardness of A356 aluminum alloy under T6 condition obtained by expendable pattern shell casting reach 260.53 MPa, 6.15% and 86.0, respectively, and obviously increase compared to as-cast condition and they are 44%, 23% and 25% higher than those of as-cast condition, respectively. Meanwhile, they have a significant improvement compared to LFC, especially in elongation.

Table 2 Quantitative metallography results for the microstructures of A356 aluminum alloy obtained from expendable pattern shell casting and LFC

Process	Expendable pattern shell casting		LFC	
	As-cast	T6	As-cast	T6
Grain size of α(Al) primary phase/μm	288.6	267.3	327.1	310.60
Secondary dendrite arm spacing (SDAS)/μm	52.37	49.20	64.15	62.24
Average length of silicon particles/μm	7.25	5.01	8.93	6.80
Average width of silicon particles/μm	3.36	2.81	3.72	3.37
Aspect ratio of silicon particles	2.16	1.78	2.40	2.02

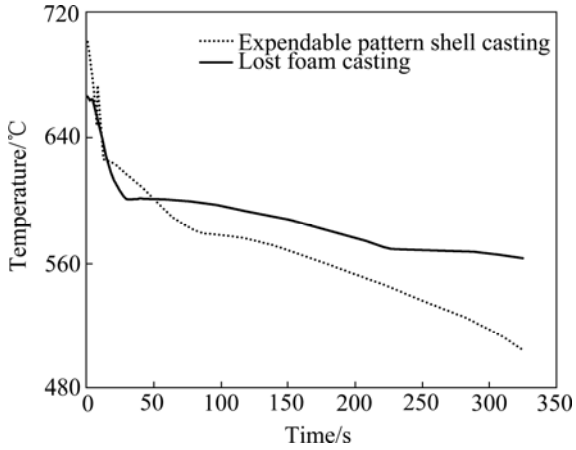

Fig. 6 Cooling curve of the molten metal during solidification for different casting processes

Table 3 Tensile properties of A356 aluminum alloy obtained with expendable pattern shell casting and LFC

Process	Expendable pattern shell casting		LFC	
	As-cast	T6	As-cast	T6
Tensile strength/MPa	180.62	260.53	148.41	231.57
Elongation/%	5.02	6.15	2.65	3.04
Hardness (HBS)	68.9	86.0	58.3	79.2

3.3 Fractography

Figure 7 shows the SEM fractographs of A356 aluminum alloy tensile samples with as-cast and T6 obtained by expendable pattern shell casting. As can be seen, the fracture surfaces of A356 aluminum alloy tensile samples with as-cast and T6 obtained by expendable pattern shell casting show a mixed quasi-cleavage and dimple morphology. Moreover, the dimple morphology of A356 aluminum alloy tensile samples under T6 condition is obvious and dispensed uniformly compared to as-cast condition, resulting in an improvement of elongation [13,14].

It can be seen from Fig. 5(a) that some elongated eutectic silicon particles are shown in the microstructure. These elongated eutectic silicon particles frequently generate fracture as they are the main sources of stress concentration [15,16]. Since some larger eutectic silicon particles cluster along both cell and grain boundaries there is a nearly continuous wall of eutectic silicon particles around the dendrite cell. The dendrite cells behave similar to grains and strong interaction between particles and slip bands generates at the cell boundaries during the plastic deformation process. Finally, the final fracture paths tend to pass through the eutectic silicon particles, and the fracture of eutectic silicon particles generates the formation of flat areas, as indicated by

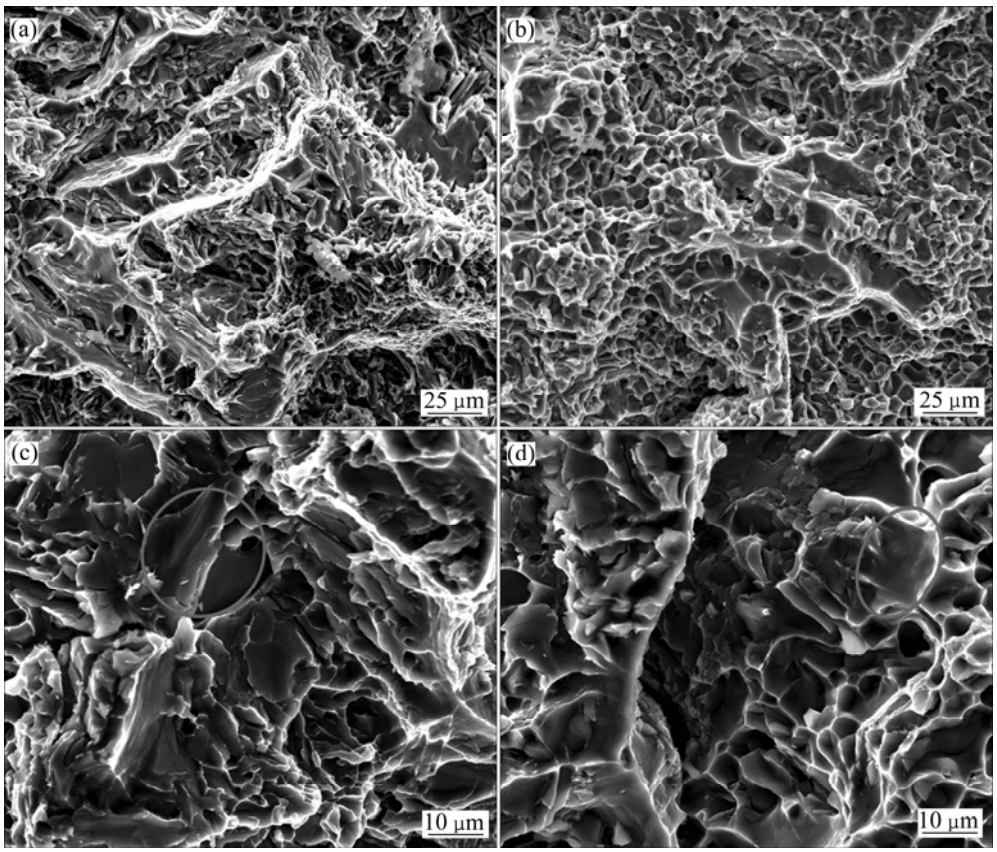

Fig. 7 SEM fractographs of A356 aluminum alloy tensile samples obtained by expendable pattern shell casting: (a) Low magnification of as-cast; (b) Low magnification of T6; (c) High magnification of as-cast; (d) High magnification of T6

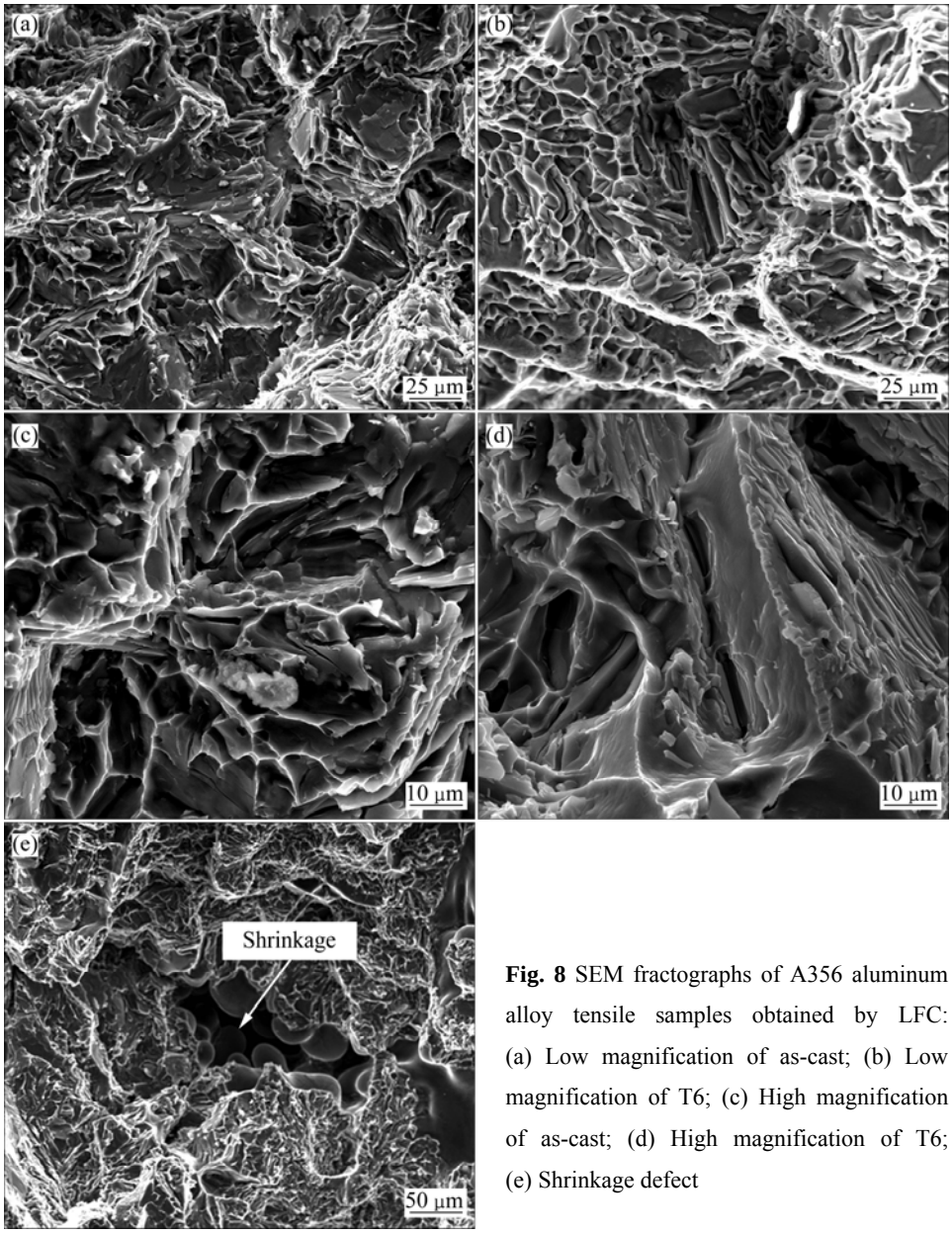

Fig. 8 SEM fractographs of A356 aluminum alloy tensile samples obtained by LFC: (a) Low magnification of as-cast; (b) Low magnification of T6; (c) High magnification of as-cast; (d) High magnification of T6; (e) Shrinkage defect

circle in Figs. 7(c) and (d). As a result, the tensile sample shows a transgranular fracture nature.

As can be seen from Fig. 8, it is evident that the fracture surfaces of A356 aluminum alloy tensile samples with as-cast and T6 produced by LFC display a clearly brittle fracture, and the quasi-cleavage feature can be observed, as shown in Fig. 8(d). Moreover, the shrinkage defects can also be observed, as shown in Fig. 8(e). The fracture path preferentially goes through the shrinkage porosity in the case of the existence of excessive shrinkage defects, which results in the significant decrease of mechanical properties.

4 Conclusions

1) α(Al) primary, eutectic silicon and Mg_2Si are the main phases in the microstructure of A356 alloy obtained with expendable pattern shell casting. The average length, average width and aspect ratio of eutectic silicon particles under T6 condition greatly decrease compared to as-cast. Furthermore, the sizes of α(Al) primary phase and eutectic silicon particles of this process are smaller than that of LFC.

2) The tensile strength, elongation and hardness of A356 alloy under T6 condition reach 260.53 MPa, 6.15% and 86.0, respectively, and they obviously increase compared to as-cast condition and are respectively 44%, 23% and 25% higher than those of as-cast condition. Moreover, they have a significant improvement compared to LFC, especially in elongation.

3) The fracture surfaces of A356 alloy tensile samples with as-cast and T6 obtained by expendable

pattern shell casting show a mixed quasi-cleavage and dimple morphology as a transgranular fracture nature. The dimple of A356 alloy samples under T6 is obvious and dispensed uniformly compared to as-cast. The fracture surfaces of LFC display a brittle fracture.

Acknowledgments

We gratefully acknowledge the test support of the Analytical & Testing Center of Huazhong University of Science and Technology (HUST).

References

[1] MöLLER H, GOVENDER G, STUMPF W E. Application of shortened heat treatment cycles on A356 automotive brake calipers with respective globular and dendritic microstructures [J]. Transactions of Nonferrous Metals Society of China, 2010, 20(9): 1780−1785.

[2] LI B, WANG H W, JIE J C, WEI Z J. Microstructure evolution and modification mechanism of the ytterbium modified Al-7.5%Si-0.45%Mg alloys [J]. Journal of Alloys and Compounds, 2011, 509(7): 3387−3392.

[3] ZHANG B, MAIJER D M, COCKCROFT S L. Development of a 3-D thermal model of the low-pressure die-cast (LPDC) process of A356 aluminum alloy wheels [J]. Materials Science and Engineering A, 2007, 464(1−2): 295−305.

[4] LI J L, CHEN R S, KE W. Microstructure and mechanical properties of Mg-Gd-Y-Zr alloy cast by metal mould and lost foam casting [J]. Transactions of Nonferrous Metals Society of China, 2011, 21(4): 761−766.

[5] LIU X J, BHAVNANI S H, OVERFELT R A. Simulation of EPS foam decomposition in the lost foam casting process [J]. Journal of Materials Processing Technology, 2007, 182(1−3): 333−342.

[6] GEFFROY P M, LAKEHAL M, GONI J, BEAUGNON E, HEINTZ J M, SILVAIN J F. Thermal and mechanical behavior of Al-Si alloy cast using magnetic molding and lost foam processes [J]. Metallurgical and Materials Transactions A, 2006, 37(2): 441−447.

[7] GRIFFITHS W D, AINSWORTH M J. Hydrogen pick-up during mould filling in the lost foam casting of Al alloys [J]. Journal of Materials Science, 2012, 47(1): 145−150.

[8] KUMAR S, KUMAR P, SHAN H S. Effect of process parameters on the solidification time of Al-7%Si alloy castings produced by VAEPC process [J]. Materials and Manufacturing Processes, 2007, 22(7−8): 879−886.

[9] ASHTON M C, SHARMAN S G, BROOKES A J. The Replicast CS (Ceramic Shell) Process [J]. Materials and Design, 1984, 5(4−5): 66−75.

[10] SHEN Gui-rong, HUANG Jing-fu, CAO JIAN, LI De-cheng, JIANG Bu-ju, YAN Shuang-jing. Study on EPC-Investment-Vacuum (EPS-CS) Compound Casting Technology and Materials [J]. Special Casting and Nonferrous Alloys, 2002(4): 54−60. (in Chinese).

[11] YUAN Zi-zhou, ZHANG Jin-song, CHEN Xiu-juan. Study on expendable pattern precision casting process. Special Casting and Nonferrous Alloys, 2003(4): 46−47. (in Chinese).

[12] RAN GUANG, ZHOU Jing-en, WANG Yong-fang, XI Sheng-qi. Microstructure and Tensile Properties of Cast A356 Aluminum Alloy [J]. Heat Treatment of Metals, 2007, 32(3): 13−18. (in Chinese).

[13] THIRUGNANAM A, SUKUMARAN K, PILLAI U T S, RAGHUKANDAN K, PAI B C. Effect of Mg on the fracture characteristics of cast Al-7Si-Mg alloys [J]. Materials Science and Engineering A, 2007, 445−446: 405−414.

[14] BAI Y F, ZHAO H D. Tensile properties and fracture behavior of partial squeeze added slow shot die-cast A356 aluminum alloy [J]. Materials and Design, 2010, 31(9): 4237−4243.

[15] WANG Q G, CACERES C H, GRIFITHS J R. Damage by eutectic particle cracking in aluminum casting alloys A356/357 [J]. Metallurgical and Materials Transactions A, 2003, 34(12): 2901−2912.

[16] FADAVI BOOSTANI A, TAHAMTAN S. Fracture behavior of thixoformed A356 alloy produced by SIMA process [J]. Journal of Alloys and Compounds, 2009, 481(1−2): 220−227.

消失模壳型铸造 A356 铸态和 T6 态铝合金的组织、性能及拉伸断口

蒋文明[1,2]，樊自田[1]，刘德均[1]

1. 华中科技大学 材料成形与模具技术国家重点实验室，武汉 430074；
2. 武汉工程大学 机电工程学院，武汉 430073

摘 要：对采用消失模壳型铸造制备的 A356 铝合金在铸态和 T6 热处理态下的微观组织、拉伸性能以及拉伸断口进行了研究，并与消失模铸造 A356 铝合金进行了对比分析。结果表明：消失模壳型铸造 A356 铝合金组织主要有 α(Al)初生相、共晶硅相以及 Mg_2Si 相组成。经过 T6 热处理后，共晶硅形貌更加球化，均匀地分布于晶界处；且共晶硅粒子的平均长度、宽度和长宽比都比铸态条件下的小。与消失模铸造相比，组织中的初生相和共晶硅相都明显细化。经 T6 处理后，消失模壳型铸造 A356 合金的力学性能得到明显提高，其中抗拉强度、延伸率和布氏硬度分别达到 260.53 MPa、6.15%和 86.0，其与消失模铸造相比具有明显优势。此外，消失模壳型铸造 A356 铝合金拉伸断口为具有准解理面和韧窝形貌的混合断口，最终表现为穿晶断裂模式。而消失模铸造 A356 铝合金拉伸断口为明显的脆性断口。

关键词：A356；微观组织；拉伸性能；断口表面；韧窝断裂；脆性断裂；消失模壳型铸造

(Edited by CHEN Can-hua)